

Interlayer transport in disordered semiconductor electron bilayers

This article has been downloaded from IOPscience. Please scroll down to see the full text article.

2012 J. Phys.: Condens. Matter 24 355301

(<http://iopscience.iop.org/0953-8984/24/35/355301>)

View [the table of contents for this issue](#), or go to the [journal homepage](#) for more

Download details:

IP Address: 128.174.190.250

The article was downloaded on 04/09/2012 at 16:20

Please note that [terms and conditions apply](#).

Interlayer transport in disordered semiconductor electron bilayers

Y Kim, B Dellabetta and M J Gilbert

Department of Electrical and Computer Engineering, University of Illinois, Urbana, IL 61801, USA
Micro and Nanotechnology Laboratory, University of Illinois, Urbana, IL 61801, USA

E-mail: matthewg@illinois.edu

Received 4 June 2012

Published 10 August 2012

Online at stacks.iop.org/JPhysCM/24/355301

Abstract

We study the effects of disorder on the interlayer transport properties of disordered semiconductor bilayers by performing self-consistent quantum transport calculations. We find that the addition of material disorder to the system affects the interlayer interactions leading to significant deviations in the interlayer transfer characteristics. In particular, we find that disorder decreases and broadens the tunneling peak, effectively reducing the interacting system to a non-interacting system. Our results suggest that the experimental observation of exchange-enhanced interlayer transport in semiconductor bilayers requires materials with mean free paths larger than the spatial extent of the system.

(Some figures may appear in colour only in the online journal)

1. Introduction

Semiconductor bilayer quantum wells have proven to be systems which exhibit an abundance of interesting physical phenomena. The bilayer system possesses both interlayer and intralayer electron–electron interaction and this additional layer degree of freedom leads to unique characteristics, especially at the half-integer filling factor, $\nu = 1/2$. When the system has equal densities of two 2DEGs with $\nu = 1/2$, the strong interlayer interaction induces spontaneous interlayer phase coherence. As a result, the system contains exotic insulating states such as exciton condensation [1, 2]. The exciton condensate transition occurs when the interlayer Coulomb interaction dominates the energy scales and its onset is signaled by a huge enhancement in the tunneling rate [1]. This exotic quantum phase transition in bilayer systems leads to a number of interesting experimental results on collective transport phenomena [3–6] which indicate that the systems may exhibit dissipationless transport [7].

While semiconductor bilayers outside of the quantum Hall regime are not expected to undergo a dramatic phase transition, theoretical investigations of interlayer exchange interaction show a number of possible ground states in bilayer systems in the absence of a magnetic field and predict a finite Coulomb drag in a low electron density regime at zero temperature [8, 9]. In addition, interlayer interactions

in a typical balanced bilayer system with zero magnetic field have been predicted to enhance the tunneling rate in a similar way to that characteristic of the quantum Hall regime, although the enhancement is orders of magnitude smaller [10]. Nevertheless, the effect of the interlayer exchange interaction can be identified experimentally by DC interlayer bias measurements [11]. While it is theoretically possible for them to be experimentally observed, these exchange-enhanced interlayer transport signatures must be robust against material disorder which these semiconductor bilayer systems are well known to contain. Therefore, an understanding of the observable deviations in interlayer transport caused by material disorder is required.

In this paper, we examine the effect of disorder on the transport characteristics of a semiconductor bilayer system in the absence of a magnetic field. The local interlayer exchange interaction is evaluated self-consistently with the proper consideration of electrostatics and the transport characteristics are obtained by the non-equilibrium Green's function (NEGF) formalism. Due to the highly screened environment of a 2DEG, only a short-range disorder is considered and the amount of disorder is modeled in terms of the mean free path (MFP) of the system [12].

Section 2 outlines the Hamiltonian and the approximations we employ to model the interlayer exchange interaction and impurities. In section 3, we present self-consistent

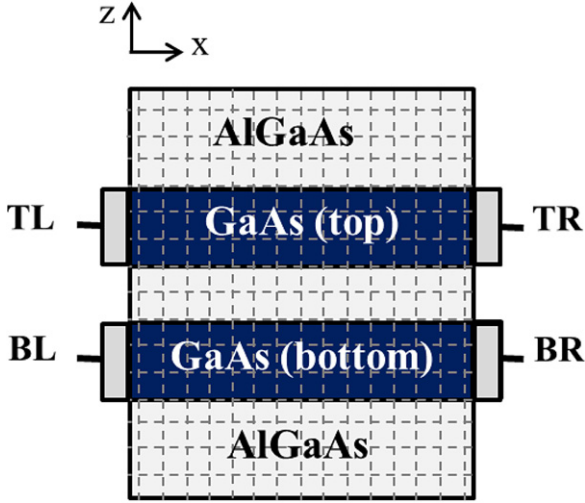


Figure 1. A schematic diagram of the $\text{Al}_{0.9}\text{Ga}_{0.1}\text{As}/\text{GaAs}$ system considered in this work.

transport results including both qualitative and quantitative analysis. As a result, as the MFP of the system becomes shorter than the device length, we find that the transport characteristics are significantly altered and the signatures of interlayer exchange interaction become increasingly difficult to observe. Finally, we summarize our results and conclude in section 4.

2. Theory

2.1. The modeling Hamiltonian

In figure 1, we plot a schematic of the system considered here. The system is comprised of two 16 nm deep GaAs quantum wells separated by a 2 nm $\text{Al}_{0.9}\text{Ga}_{0.1}\text{As}$ barrier. The gates on the top and bottom are isolated from their respective quantum wells by 60 nm thick top and bottom $\text{Al}_{0.9}\text{Ga}_{0.1}\text{As}$ barriers. Contacts inject and extract electrons from the system on the left and right ends of both the top and bottom layers. We use the tunneling bias configuration ($V_{\text{TL}} = V_{\text{TR}} = V_{\text{BL}} = 0$, $V_{\text{BR}} = V_{\text{INT}}$) in which electrons are injected into the bottom right contact and are extracted from the top left contact. The length and width of the system are each $1.2 \mu\text{m}$ and we assume that each 2DEG contains an electron concentration of $n_{2\text{D}} = 3 \times 10^{10} \text{ cm}^{-2}$. The system temperature for all of our simulations is set to the zero temperature limit, or $T_{\text{sys}} = 0 \text{ K}$.

We define the single quantum well Hamiltonian of the top (t) and bottom (b) layers as

$$H_{\text{t(b)}} = \sum_{\langle i,j \rangle} -\tau |i\rangle \langle j| + (4\tau + V_i) |i\rangle \langle i|, \quad (1)$$

where the lattice points i and j are nearest neighbors. $\tau = \hbar^2/2m^*a^2$ is the nearest neighbor hopping energy, where m^* is the electron effective mass of GaAs and $a = 20 \text{ nm}$ is the lattice constant of our simulation. $V_i = \phi(\mathbf{r}_i)$ is the on-site potential for GaAs from the normal tight-binding description and is calculated via a three-dimensional Poisson solver. We

may now generalize our 2DEG Hamiltonian to the double quantum well Hamiltonian by coupling the top and bottom quantum 2DEGs [11, 13],

$$\mathcal{H}_{\text{sys}} = \begin{bmatrix} H_t & 0 \\ 0 & H_b \end{bmatrix} + \sum_{\mu=x,y,z} \hat{\mu} \cdot \Delta \otimes \sigma_{\mu}, \quad (2)$$

where μ represents a vector that isolates each of the Cartesian components of the pairing vector and σ_{μ} represents the Pauli spin matrices in each of the three spatial directions. In equation (2), the first term on the right-hand side corresponds to the Hamiltonian of each individual quantum well and the second term includes interlayer interactions from both single particle tunneling and the mean-field many-body contribution. Considering that the electron interaction is highly screened in a 2DEG, we use a local density approximation and only consider on-site interlayer interaction. As a result, each component of Δ in equation (2) is described using a typical mean-field decomposition as

$$\begin{aligned} \Delta_x &= -t + U\langle m_x \rangle, \\ \Delta_y &= U\langle m_y \rangle, \\ \Delta_z &= (V_t - V_b)/2. \end{aligned} \quad (3)$$

In equation (3), we use $t = 2 \mu\text{eV}$ as the single particle tunneling amplitude and $V_{\text{t(b)}}$ is the on-site Hartree potential of the top (bottom) layer. The exchange interaction, $U\langle m_{x,y} \rangle$, can be obtained from the single particle density matrix as

$$\begin{aligned} \langle m_x \rangle &= (\rho_{\text{t,b}} + \rho_{\text{b,t}})/2, \\ \langle m_y \rangle &= (-i\rho_{\text{t,b}} + i\rho_{\text{b,t}})/2, \end{aligned} \quad (4)$$

where $\rho_{\text{b,t(t,b)}}$ is the off-diagonal contribution to the density matrix

$$\rho = \begin{bmatrix} \rho_t & \rho_{\text{t,b}} \\ \rho_{\text{b,t}} & \rho_b \end{bmatrix}. \quad (5)$$

The diagonal terms of the density matrix (ρ_t, ρ_b) are the electron densities of the top and bottom layers. We model the exchange interaction constant, U in equation (3), using an enhancement factor S , so that the resultant quasi-particle tunneling amplitude becomes $t_{\text{eff}} = St$ [10]. Using the local density approximation, U satisfies

$$U = \frac{1 - S^{-1}}{\nu_0}, \quad (6)$$

where $\nu_0 = m^*/\pi\hbar^2$ is the two-dimensional density of states¹. In equation (6), S is the exchange–correlation enhancement of the tunneling amplitude t which is similar to the enhancement of exchange in the Stoner criterion for itinerant ferromagnetism. In the limit of vanishing tunneling $t \rightarrow 0$, the Stoner interaction parameter, $I = 1 - S^{-1}$, is defined using a variational Hartree–Fock-like approximation as [8]

$$I = \frac{\nu_0 e^2}{2\pi\epsilon k_{\text{F}}} \left(1 - \frac{1}{2} \int_0^{\pi/2} d\theta \frac{1 - e^{-2k_{\text{F}}d \sin \theta}}{\sin \theta} \right), \quad (7)$$

¹ More details of the procedure to reach equation (6) are outlined in [11].

where ϵ is the dielectric constant, $k_F = \sqrt{2\pi n_{2D}}$ is the Fermi wavevector and d is the interlayer separation. Although the enhancement factor, S , is a function of the layer separation and electron density, the physically relevant range of the enhancement factor should be small [8, 10], as we do not expect spontaneous coherence in this system. For example, when $\epsilon = \epsilon_{\text{GaAs}} = 12.9\epsilon_0$, $n_{2D} = 3 \times 10^{10} \text{ cm}^{-2}$ and $d = 18 \text{ nm}$, the enhancement factor calculated from equation (7) is $S \simeq 1.40$. As the physics behind the exchange interaction of the system is still valid as long as the value of S is small, we use $S = 2$ for the remainder of this work when discussing interacting bilayer systems.

2.2. Modeling of the disorder

To understand the effects of material disorder in the GaAs/AlGaAs system [12], the impurities are assumed to be highly screened in the 2DEG. As a result, the impurity potential may be described as a δ -function. Within a lattice model, random disorder can be inserted into the system Hamiltonian by adding a uniform distribution having an energy window of W to the on-site energy. Then, the on-site energy in the disordered system satisfies the inequality $-W/2 \leq \epsilon_i - \epsilon_0 \leq W/2$, where $\epsilon_{i(0)}$ is the on-site energy of the system with (without) disorder. The W in a two-dimensional lattice model containing high concentrations of δ -function impurities satisfies the relationship [12]

$$\frac{W}{E_F} = \left(\frac{6\lambda_F^3}{\pi^3 a^2 \Lambda} \right)^{1/2}, \quad (8)$$

where E_F , λ_F are the Fermi energy and Fermi wavelength, respectively, and a is the lattice constant. Consequently, the impurity level is characterized by a mean free path (MFP), Λ . At a given MFP, the random impurities act as rigid scatterers and alter the on-site potential of the device according to equation (8). The effect of these scatterers on the electron propagation is evaluated in the limit of coherent transport, as there is no phase-breaking mechanism included (e.g. phonon scattering) [14]. Therefore, the current may be calculated via the Landauer formula as has been done in previous studies of Si [15] and graphene nanoribbons [16].

2.3. Simulation detail

The calculation strategy follows a standard self-consistent field procedure. We evaluate the mean-field quasi-particle Hamiltonian with the non-equilibrium Green's function (NEGF) formalism [14] coupled with a 3D Poisson equation. The effective interlayer interaction, Δ , is also updated during the loop, which proceeds until a desired level of self-consistency is achieved. When the MFP is larger than the system length, there is no significant modification to the interlayer transport. Thus, we only focus on an MFP comparable to or smaller than the device size. When the MFP is comparable to the device size, however, the many-body contribution to Δ shows local fluctuations around the region where the on-site potential is significantly modified. As this

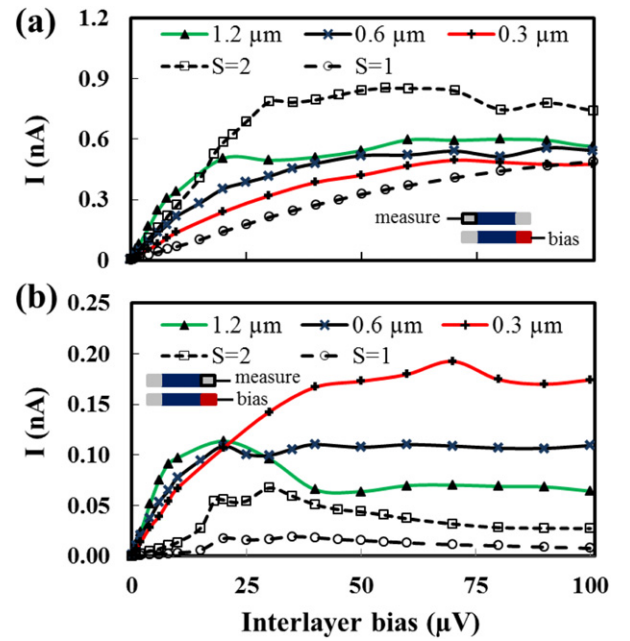


Figure 2. A plot of current as a function of interlayer bias for electrons injected into the bottom right contact and extracted from (a) the top left contact and (b) the top right contact. The error bar is omitted for visual clarity.

numerical fluctuation is not critical for global observables and depends on the particular disorder configuration, the data obtained from the simulation are averaged over ten different disorder configurations in order to mitigate the numerical fluctuations.

3. Results and discussion

In figures 2(a) and (b), we analyze the I - V characteristics of the disordered system sweeping the interlayer bias up to $V_{\text{INT}} = 100 \mu\text{V}$. We now introduce impurities into the system corresponding to three different MFPs of $\Lambda = 1.2, 0.6$ and $0.3 \mu\text{m}$. The range of MFPs we consider here adds a significant perturbation to the on-site energy of 10–20% of the self-consistent Hartree potential. In figure 2(a), we plot the current flowing from the bottom right contact (BR) to the top left contact (TL) and immediately see the effects of disorder. By comparing the interacting ($S = 2$) and non-interacting ($S = 1$) systems, we notice that the interacting system has a uniform current enhancement over the non-interacting case over all interlayer voltages. However, when disorder corresponding to an MFP commensurate with the system size is introduced, we see that the interlayer current is increased at low V_{INT} . This is a consequence of local regions of stronger interlayer interactions set up by disorder-induced localization. As V_{INT} is increased, the interlayer enhancement quickly disappears and leaves only a small exchange enhancement over the non-interacting case. As the MFP is further decreased, we see that the trend of decreased interlayer exchange enhancement continues as the perturbations to the carriers via the disorder potential are now large enough to energetically separate

the two layers leaving only weak interlayer interactions. A separate way of visualizing the effects of disorder is via figure 2(b), where we plot the current injected from the bottom right (BR) contact and extracted from the top right contact (TR). Here, we would expect the interlayer current to be close to zero as we see for the $S = 1$ and 2 cases without disorder. However, when disorder localizes the electron states in the bottom layer, the interlayer tunneling is locally enhanced, leading to increased interlayer transmission near the injection contact. Beyond locally enhanced transmission, the presence of disorder in the top layer perturbs the electron states leading to backscattering of injected states. The overall effect is an increasing current from BR to TR as the disorder increases.

A crucial component to understanding the interlayer dynamics in the presence of material disorder is the critical current (I_c), or amount of interlayer current the system can sustain by simply altering the interlayer phase. As we have not passed a phase boundary, we do not expect large differences in interlayer currents between before and after the critical current. In the system without disorder, the critical current from the simulation is $I_c^{\text{clean}} = 0.89$ nA, which is smaller than the predicted critical current [11] of $I_c^{\text{anal}} = 3.14$ nA.² This discrepancy can be understood by considering the charge imbalance of two layers. As the bottom layer is biased, the charge imbalance builds up the electrostatic potential across the two layers. When the charge imbalance between the layers is sufficiently large, the two nested Fermi surfaces are separated. As a result, the interlayer current is decreased before the system reaches the critical current. We calculate a critical current for each disorder configuration and MFP and find that $I_c^{1.2 \mu\text{m}} = 0.86 \pm 0.10$ nA, $I_c^{0.6 \mu\text{m}} = 0.73 \pm 0.05$ nA and $I_c^{0.3 \mu\text{m}} = 0.75 \pm 0.05$ nA, all of which are smaller than the disorder free case. We find that the critical current saturates with increasing disorder but this is simply because the exchange enhancement has been lost and the system responds as if it is non-interacting for MFPs shorter than the system dimensions.

The effect of disorder can be quantitatively analyzed by probing the interlayer conductance. Figures 3(a)–(c) depict the tunneling conductance which is defined as $G = (I_{\text{TL}} + I_{\text{TR}})/V_{\text{INT}}$. We find that the width of the tunneling conductance peak broadens with increasing material disorder. With a given MFP, the broadening (Lorentzian half-width, Γ) is calculated as [17] $\Gamma = \frac{\hbar}{\tau}$, where τ is the quantum lifetime of the electrons. The predicted broadenings ($\Gamma/2$) for $\Lambda = 1.2, 0.6, 0.3 \mu\text{m}$ are $\sim 20, 41, 82 \mu\text{eV}$, respectively. Our results show energy broadenings of $20.6 \pm 2.4, 31.9 \pm 4.4, 64.2 \pm 7.5 \mu\text{eV}$, respectively, in good agreement with the predicted values. For a disordered system which has a well balanced electron density and satisfies $E_f \gg \Gamma$, the calculated interlayer conductance, G , is described as [18]

$$\frac{G}{A} = \frac{2e^2 t^2 v_0 \tau}{\hbar^2} = \frac{2e^2 t^2 v_0}{\hbar^2 v_f} \Lambda, \quad (9)$$

where A is the system area, t is the tunneling amplitude and $v_0 = m^*/\pi \hbar^2$ is the two-dimensional density of states.

² The critical current can be calculated from equation (20) of [11] using the fact that $|\mathbf{m}_{\mathbf{xy}}| = v_0 S t$ in a well balanced bilayer system.

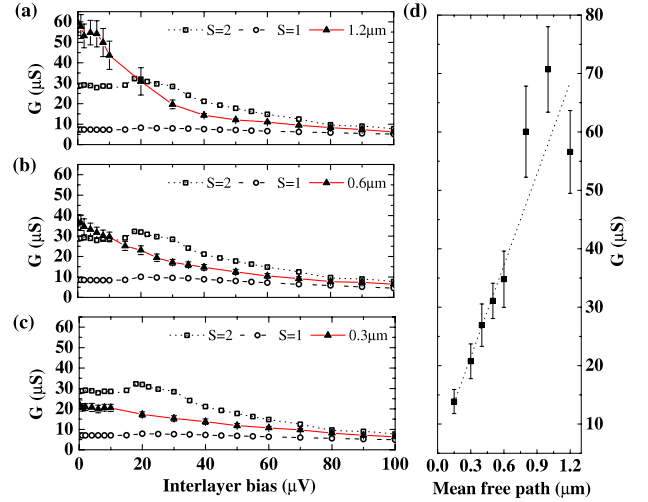


Figure 3. Plots of the interlayer conductance, G , as a function of the interlayer bias with mean free paths of (a) $1.2 \mu\text{m}$, (b) $0.6 \mu\text{m}$ and (c) $0.3 \mu\text{m}$. (d) Plot of the maximum height of the interlayer conductance as a function of the mean free path at $V_{\text{INT}} = 0.1 \mu\text{V}$. The plots of (a)–(c) are presented by averaging over ten different disorder configurations and the plot (d) is presented by averaging over six different disorder configurations.

Equation (9) reveals a linear dependence of the conductance on the MFP. In figure 3(d), we plot the interlayer conductance as a function of the MFP at the bias point where the two layers are well balanced ($V_{\text{INT}} = 0.1 \mu\text{V}$). We observe a linear dependence in the interlayer conductance, especially at MFPs shorter than $\Lambda = 0.6 \mu\text{m}$. The broadening in the tunneling peak and the linear dependence of the interlayer conductance on the MFP indicate that the interlayer transport is no longer controlled by the intrinsic nature of the system and is instead controlled by the material disorder when the MFP is shorter than the device length.

As important as it is to understand the variations in the magnitude of the interlayer current, we must also understand how disorder shifts the local interlayer current flow. In figure 4, we plot the spatially resolved interlayer current profile below and above the critical current for a clean system (left column) and one with an MFP of $\Lambda = 0.3 \mu\text{m}$ (right column). In the linear response regime, the interlayer transmission probability of the channel k is proportional to v_k^{-2} , where v_k is the quasi-particle Fermi velocity of the channel k in the transport direction [11]. The quasi-particle subband with the highest transverse velocity, or the highest quantized energy level, has the lowest longitudinal velocity and, consequently, makes the largest contribution to interlayer transport. As a result, the quasi-particle wavefunction of the highest quantized level contributes most significantly to the tunneling current. The effect is manifested as a transverse directional oscillation in the current profile in figure 4 due to the small degree of confinement in our $1.2 \mu\text{m}$ wide structure. In the clean case, we see in figure 4(a) that the interlayer current density is peaked near the contacts at small interlayer bias. This is clearly not the case in figure 4(b), where we see that above the critical current the clean system exhibits an even spatial distribution of the interlayer current.

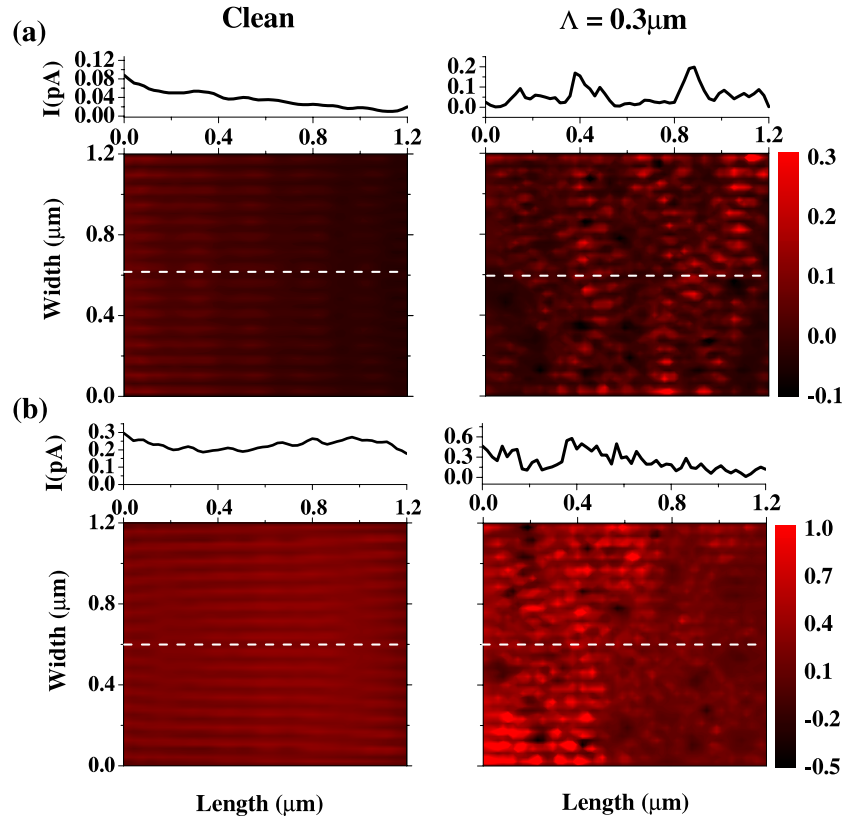


Figure 4. A plot of the spatially resolved current as a function of device width and length at (a) $V_{\text{INT}} = 10 \mu\text{V}$ and (b) $V_{\text{INT}} = 80 \mu\text{V}$ in units of pA for an assumed enhancement factor of $S = 2$. The current profile of the clean system (disordered system of $\Lambda = 0.3 \mu\text{m}$) is presented in the left (right) column. Above each two-dimensional plot, there is a current profile taken in the middle of the system indicated as a white dashed line.

In the presence of strong disorder, however, the interlayer current flows randomly across the system. The current profile of the disordered system has been broken up into regions of strong and weak single particle interlayer current flow controlled by the disorder pattern in both the small and large bias cases. Even though the current profile is arbitrarily distributed, the regions where the tunneling is strongly suppressed are independent of the interlayer bias as is shown in the right column of figure 4 (dark regions). Meanwhile, there is a significant difference in the current flow profile from different disorder configurations, which further indicates the strong dependence of the current flow on the disorder configuration. The net current averages out the locally enhanced and suppressed current flows and results in a smaller current than that of the clean system. This gives further evidence that the disorder controls the interlayer transport properties when the corresponding MFP is smaller than the system dimensions.

4. Conclusion

In conclusion, we have shown that while exchange-enhanced interlayer transport properties in semiconductor bilayers may exist outside the quantum Hall regime, they are very sensitive to the strength and location of material disorder. We find that as soon as the MFP of the electrons becomes commensurate

with the spatial system dimensions, the disorder controls the interlayer transport properties and reduces the interacting electron system to a non-interacting one. These findings demonstrate that to observe these states experimentally one requires systems with MFPs greater than the system spatial dimensions.

Acknowledgments

This work is supported by the Army Research Office (ARO) under Contract No. W911NF-09-1-0347. We acknowledge support for the Center for Scientific Computing from the CNSI, MRL: an NSF MRSEC (DMR-1121053) and NSF CNS-0960316 and Hewlett-Packard. Y Kim is supported by Fulbright Science and Technology Award.

References

- [1] Eisenstein J P and MacDonald A H 2004 *Nature* **432** 691
- [2] Moon K, Mori H, Yang K, Girvin S M, MacDonald A H, Zheng L, Yoshioka D and Zhang S-C 1995 *Phys. Rev. B* **51** 5138
- [3] Spielman I B, Eisenstein J P, Pfeiffer L N and West K W 2000 *Phys. Rev. Lett.* **84** 5808
- [4] Kellogg M, Spielman I B, Eisenstein J P, Pfeiffer L N and West K W 2002 *Phys. Rev. Lett.* **88** 126804
- [5] Tiemann L, Yoon Y, Dietsche W, von Klitzing K and Wegscheider W 2009 *Phys. Rev. B* **80** 165120

- [6] Yoon Y, Tiemann L, Schmult S, Dietsche W, von Klitzing K and Wegscheider W 2010 *Phys. Rev. Lett.* **104** 116802
- [7] Su J-J and MacDonald A H 2008 *Nature Phys.* **4** 799
- [8] Hanna C B, Haas D and Diaz-Velez J C 2000 *Phys. Rev. B* **61** 13882
- [9] Zheng L, Ortalano M W and Das Sarma S 1997 *Phys. Rev. B* **55** 4506
- [10] Swierkowski L and MacDonald A H 1997 *Phys. Rev. B* **55** R16017
- [11] Kim Y, MacDonald A H and Gilbert M J 2012 *Phys. Rev. B* **85** 165424
- [12] Ando T and Tamura H 1992 *Phys. Rev. B* **46** 2332
- [13] Gilbert M J 2010 *Phys. Rev. B* **82** 165408
- [14] Datta S 2005 *Quantum Transport: Atom to Transistor* (Cambridge: Cambridge University Press)
- [15] Martinez A, Barker J R, Seoane N, Brown A R and Asenov A 2010 *J. Phys.: Conf. Ser.* **220** 012009
- [16] Sui Y, Low T, Lundstrom M and Appenzeller J 2011 *Nano Lett.* **11** 1319
- [17] Turner N, Nicholls J T, Linfield E H, Brown K M, Jones G A C and Ritchie D A 1996 *Phys. Rev. B* **54** 10614
- [18] Zheng L and MacDonald A H 1993 *Phys. Rev. B* **47** 10619